Mineralogical Magazine, May 2018, Vol. 82(S1), pp. S259–S279

Fe-, Fe,Mn- and Fe,Mg-chlorite: a genetic linkage to W, (Cu, Mo) mineralization in the magmatic-hydrothermal system at Borralha, northern Portugal

I. Bobos[1,*], F. Noronha[1] and A. Mateus[2]

[1] Instituto de Ciências da Terra – Polo Porto, Departamento de Geociências, Ambiente e Ordenamento do Território, Faculdade de Ciências, Universidade do Porto, Rua do Campo Alegre 687, 4169-007 Porto, Portugal

[2] Departamento de Geologia e IDL, Faculdade de Ciências, Universidade de Lisboa, C6, Campo Grande, 1746-016 Lisboa, Portugal

[*Received 23 January 2017; Accepted 22 December 2017; Associate Editor: Krister Sundblad*]

ABSTRACT

A genetic linkage between W, (Cu, Mo)-mineralization and chlorite minerals, and the discrimination of different mineralization events in the magmatic-hydrothermal system of Borralha, northern Portugal, is discussed on the basis of textural relationships, crystal chemistry and stable isotopic data obtained from chlorite. Chlorite minerals were identified in assemblages with quartz, feldspars, tungstates and sulfides. X-ray diffraction studies of selected chlorite minerals shows a trioctahedral structural type. Electron probe micro-analyses identified four different compositions and associations: (1) Fe,Mn-chlorite with scheelite I; (2) Fe-chlorite with wolframite + scheelite II ± sulfide; (3) Fe,Mg-chlorite with molybdenite + bismuthinite; and (4) Mg,Fe-chlorite with chalcopyrite. The composition of Fe-chlorite $(Al_{3.01}Fe^{3+}_{0.25}Fe^{2+}_{7.95}Mn_{0.26}Mg_{0.19})_{11.66}(Si_{5.44}Al_{2.56})_8O_{20}(OH)_8$ corresponds to daphnite and Fe,Mn-chlorite $(Al_{2.69}Fe^{3+}_{0.02}Fe^{2+}_{7.54}Mn_{1.08}Mg_{0.62})_{11.89}(Si_{5.31}Al_{2.68})_4O_{20}(OH)_8$ to a mixed composition between daphnite and amesite. The Fe,Mg-chlorite $(Al_{2.89}Fe^{3+}_{0.24}Fe^{2+}_{6.42}Mn_{0.21}Mg_{2.08})_{11.84}$ $(Si_{5.31}Al_{2.79})_8F_{0.31}O_{20}(OH)_8$ corresponds to ripidolite and Mg,Fe-chlorite $(Al_{2.63}Fe^{3+}_{0.37}Fe^{2+}_{1.72}Mn_{0.01}Mg_{6.40}Ca_{0.26})_{11.39}(Si_{6.02}Al_{1.98})_8O_{20}(OH)_8$ to pychnochlorite.

Chlorite geothermometry estimates a temperature for Fe,Mn-chlorite (scheelite I) from 400°C to 500°C, for Fe-chlorite (Mn-rich wolframite + scheelite II ± sulfide) from 250 to 350°C, for Fe,Mg-chlorite (Mo-mineralization) from 200°C to 250°C and for Mg,Fe-chlorite at ~150°C. Oxygen isotopes (V-SMOW) yielded values of +3.8 (1σ) (Fe-chlorite), +6.91 (1σ) (Fe,Mn-chlorite) and +1.5 (1σ) (Fe,Mg-chlorite). The calculated $\delta^{18}O_F$ of Fe- and Fe,Mg-chlorite is ~+3.75 (1σ) and +1.45 (1σ) for the mineralizing fluid, whereas for Fe,Mn-chlorite it is +8.17 (1σ). The $\delta^{18}O$ data obtained from quartz in W- and Mo-mineralization yielded values of +12.6 and +11.4 (1σ), whereas for adularia $\delta^{18}O$ is about +10 (1σ). These estimates allow us to conclude that the Fe,Mn-chlorite crystallized from a magmatic-hydrothermal fluid, whereas the Fe- and Fe,Mg-chlorite quartz and adularia resulted from a mixed contribution between meteoric and magmatic-hydrothermal fluid.

*E-mail: ibobos@fc.up.pt

https://doi.org/10.1180/minmag.2017.081.104

Keywords: chlorite, tungstates and sulfides, crystal chemistry, geothermometry, oxygen isotopes, Borralha, Portugal.

This paper is part of a special issue entitled 'Critical-metal mineralogy and ore genesis'. The Applied Mineralogy Group of the Mineralogical Society and the IMA Commission on Ore Mineralogy have contributed to the costs of Open Access publication for this paper.

Introduction

THE metallogenic processes intimately associated with a variety of late- to post-magmatic events are sometimes poorly understood in detail due to a wide compositional diversity of the fluids involved in metal transport and deposition, where the late silicate phases may be an indicator of a distinct stage of mineralization. One of the most common late silicate phases is chlorite. It is frequently found either in hydrothermal alteration haloes that host ores or accompanying the ore-forming phases. The chlorite represents an alteration product following the breakdown of different primary minerals as the H^+ or Mg^{2+},Fe^{2+}-metasomatism proceeds. These reactions are usually related to propylitic alteration (i.e. actinolite + epidote + chlorite or epidote + chlorite + calcite or chlorite + calcite + hematite assemblages). The reactions are quite common and well developed in a wide range of ore-forming systems, including iron-oxide copper gold, porphyry Cu, Cu-Mo or Cu-Au, epithermal Au-Ag, and retrograde alteration stages of skarn-type deposits (e.g. Lowell and Guilbert, 1970; Gustafson and Hunt, 1975; Meinert, 1992; Sillitoe, 2000, 2010; Cooke *et al*., 2014). The chemical composition of chlorites from the distal fringes of hydrothermal envelopes is distinct from that characteristic of metamorphism.

The wide range of crystal chemistry and structure displayed by the chlorite minerals group may also be used as a tool to determine the direction towards the mineralized area, to estimate the temperature under which the ore process took place (e.g. Cathelineau and Nieva, 1985; Walshe, 1986; Inoue *et al*., 2010) or to estimate the heat flux from a magmatic-hydrothermal centre (Sillitoe, 2010). Recently, the relationships 'chlorite vs. metal assemblages' were revisited and explored to use chlorite as a proxy for detecting porphyry ore deposits (Wilkinson *et al*., 2015).

Dispersion or remobilization of metals in long-lived magmatic hydrothermal systems occurs *via* circulation of compositionally diverse fluids under a relatively large range of temperatures, generating useful environmental markers when ore-forming minerals are deposited with other phases such as chlorite. When precipitated directly from the hydrothermal fluid, chlorite displays a chemical composition that reflects many of the constraints imposed by the fluid chemistry during mineralization. For example, a genetic linkage between Mg, Fe-chlorite or Fe,Mg-chlorite and Cu-Au mineralization (Dora and Randive, 2015) or a Pb-Zn, Bi, Ag vein-type ore deposit (Inoue *et al*., 2010) has been established. Beside the relative enrichment of Fe or Mg in the octahedral sheet in chlorite, the systematic presence of measurable amounts of Mn has been tested as a new pathfinder for chlorite developed during an ore-forming processes. For instance, Fe,Mg,Mn-chlorite has been identified in Pb-Zn, Bi, Ag ore veins from the Toyoha geothermal system, Japan (Inoue *et al*., 2010), and Fe,Mn,Mg-chlorite was recognized in the Zn-Pb, Ag vein-type ore epithermal system in NE Chile (Chinchilla *et al*., 2016).

The main goal of the present contribution is to characterize the optical, structural and crystal chemistry of chlorite minerals associated with tungstate and sulfide mineralization from the W, (Cu,Mo) ore deposit of Borralha (Portugal). The relationships between the development of chlorite minerals and different ore-forming stages as well as discrimination of different mineralization events based on stable isotopic studies of chlorite minerals are addressed.

Geology

The Variscan orogeny is an obduction-collision orogenic event (e.g. Ribeiro *et al*. 1990, 2007; Matte, 1991), where three main deformation phases (D1, D2 and D3) have been documented in northern Portugal (Ribeiro, 1974; Noronha *et al*., 1981). The maximum crustal thickening was achieved by the end of D1/D2 phases, whereas the D3 phase (intra-Westphalian age) relates to the final stages of the continental collision process. Most of the granite intrusions and the associated thermal metamorphic peak are coeval with the D3 phase (e.g. Ferreira *et al*., 1987; Dias and Ribeiro, 1995; Noronha *et al*., 2000; Ribeiro *et al*., 2007). The syn- to late-orogenic magmatic activity generated voluminous granitoid batholiths, often with contrasting compositions, and the emplacement was, in most cases, controlled by major Variscan structures.

The W, (Cu,Mo) deposit of Borralha is located in the northwestern Iberian Peninsula near the boundary between the Central Iberian Zone and the Galicia Trás-os-Montes subzone (Fig. 1), where different synorogenic Variscan granites intrude Palaeozoic metasedimentary rocks to form two-mica peraluminous (syn-D3) granites and biotite-rich (syn-D3) granites. The ore deposit occurs at the contact between metasedimentary formations (Silurian?) and the syn-D3 porphyritic Borralha biotite granite (~315 Ma) and a syn-D3 two-mica

https://doi.org/10.1180/minmag.2017.081.104 Published online by Cambridge University Press

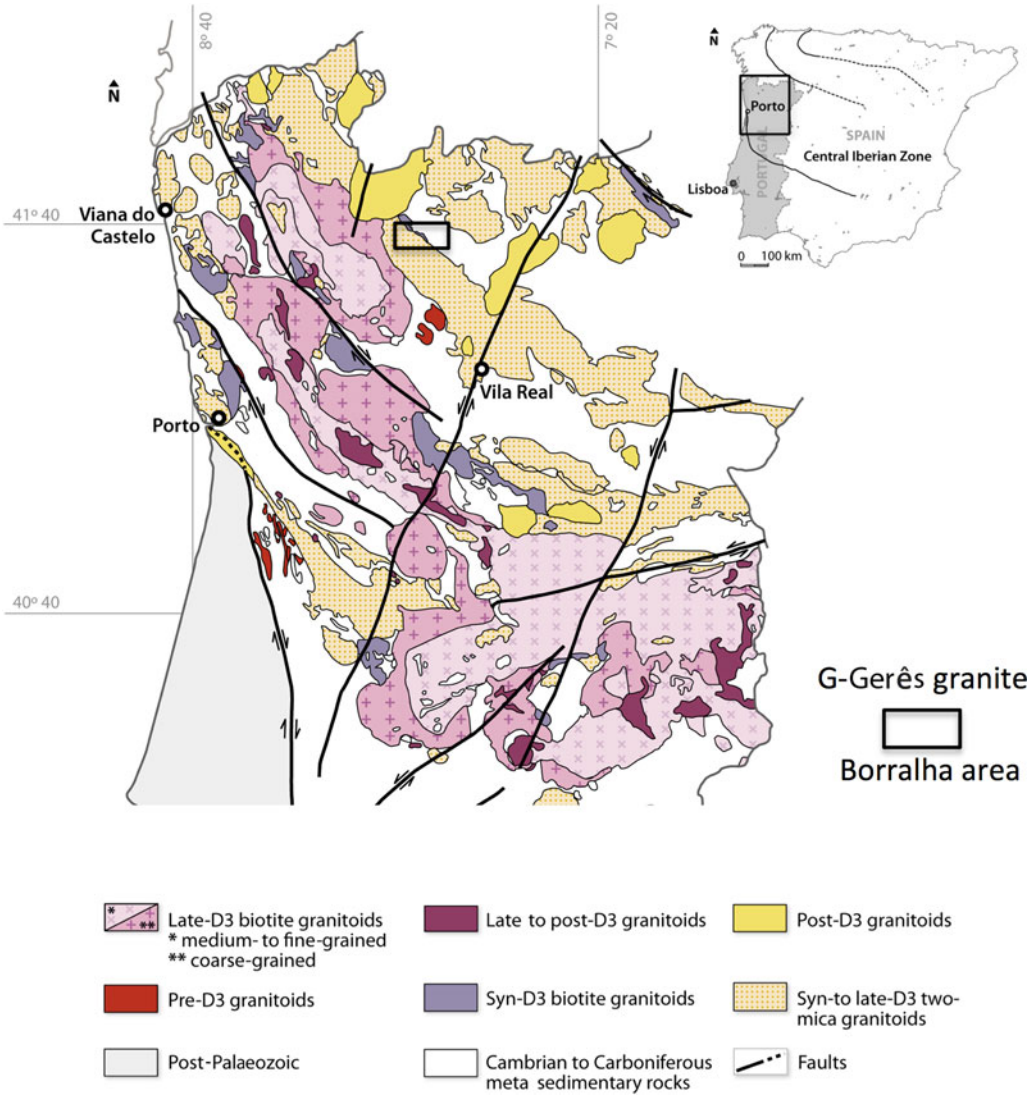

FIG. 1. Geological map of the northern part of Portugal showing the location of the W, (Cu,Mo) ore deposit of Borralha, Gerês Mountains (after Ferreira *et al*., 1987).

granite (Fig. 2) assumed to be related to a concealed post-D3 granite body (i.e. the Gerês granite).

Petrogenetic and petrophysical studies of the post-D3 Gerês granite show that the magma rose relatively high in the crust and settled at upper crustal levels (6–7 km), generating a temperature gradient which triggered contact metamorphism at 200 MPa and 500–600°C which was sufficient to promote a vigorous hydrothermal convection cell (Noronha and Ribeiro, 1983; Noronha *et al*., 2000).

The Borralha ore deposit is an important tungsten deposit of Portugal second only to Panasqueira. It was mined from 1903 to 1985 for wolframite, scheelite and argentiferous chalcopyrite. The mineralization occurs in quartz veins and in the two breccia pipes known as Santa Helena and Venise. The Santa Helena breccia occurs in outcrop (Fig. 2), whereas the Venise breccia was identified underground during mining. Rock fragments of variable size, cemented with mineralized

https://doi.org/10.1180/minmag.2017.081.104 Published online by Cambridge University Press

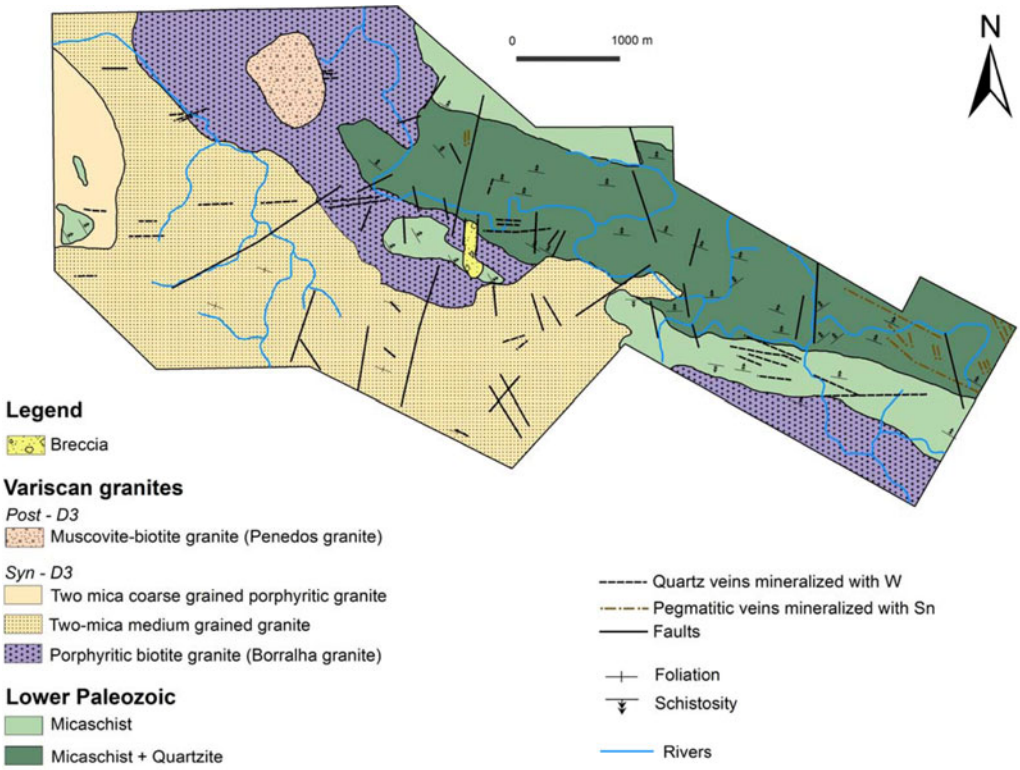

FIG. 2. Geological map of the Borralha region (after Noronha, 1983).

coarse-grained quartz aggregates, characterize both breccias. Shallow levels of the Santa Helena breccia were mined for tungsten (i.e. wolframite). The ore mineral assemblage consists of tungstate (wolframite and scheelite), various sulfide minerals (chalcopyrite + molybdenite and pyrite, pyrrhotite, sphalerite, galena, bismuthinite, marcasite), native bismuth and Pb-Bi-Ag sulfosalts. Fluid-inclusion studies of quartz related to the W-mineralization identified aqueous-carbonic fluids ($300°C < T < 400°C$ and $50\ MPa < P < 100\ MPa$) and aqueous fluids ($250°C < T < 300°C$ and $30\ MPa < P < 50\ MPa$) in sulfide mineralization (Noronha, 1984*a*; Noronha *et al*., 1999).

Other lode-quartz systems carrying W-Mo, (Sn) mineralization were described at Carris and Las Sombras (20 km NNW of Borralha), and are assumed to be related to the post-D3 Gerês granite (Cheilletz and Giuliani, 1982; Noronha, 1983, 1984*a*). An integrated metallogenic model was proposed by Noronha (1984*a*) with four progressive stages of magmatic-hydrothermal evolution of the post-D3 Gerês granite: (1) Mo, (W) at Bouzadrago (Galicia, Spain); (2) W-Sn, (Cu, Mo,Bi) at Las Sombras (Galicia, Spain), Carris and Borrageiro; (3) W, (Cu,Mo,Bi,Sn) at Penedos; and (4) W, (Cu,Mo,Bi) at Borralha.

K-Ar dating of muscovite associated with molybdenite from the Venise breccia provided an age of 280 ± 5 Ma (Portugal-Ferreira and Noronha, unpublished data). K-Ar dating of feldspar from episyenitic rocks of the Gerês granite (Carris facies) yielded an age of 273 ± 11 Ma (Jaques *et al*., 2016), whereas Re-Os dating of molybdenites from Carris quartz veins placed the ore-forming stage at 279.5 ± 1.7 (Moura *et al*., 2014).

Samples and analytical techniques

Samples

Samples containing tungstates and Cu-,Zn-,Bi-sulfides were collected from three drill cores (at −40 m; −70 m; −176 m levels) of the Santa Helena

https://doi.org/10.1180/minmag.2017.081.104 Published online by Cambridge University Press

breccia where the chlorite *vs*. mineralization occurs unambiguously at different scales. Representative samples of chlorite associated with Mo-mineralization were collected from the Venise breccia at the −110 m level. Illustrative features of these samples are: (1) a Fe,Mg-chlorite with quartz, albite and adularia assemblage (Fig. 3*a*); (2) Fe,Mn-chlorite with scheelite (Fig. 3*b*); (3) Fe-chlorite with W-mineralization (Fig. 3*c*); (4) Fe-chlorite with chalcopyrite + sphalerite ± pyrite and secondary muscovite (Fig. 3*d*); and (5) Fe,Mg-chlorite with molybdenite (adularia + quartz) (Fig. 3*e*). Fractions of Fe,Mg-chlorite (Fig. 3*a*) with quartz, albite and adularia (compositionally identical to Fe, Mg-chlorite with molybdenite), Fe-chlorite (Fig. 3*d*) and Fe,Mn-chlorite (Fig. 3*b*) were separated and used further in X-ray diffraction (XRD), optical microscopy, electron microprobe analyses (EMPA) and oxygen isotopic measurements. The samples involving chlorite + tungstates and chlorite + sulfides were studied by optical microscopy and EMPA and special attention was given to the chlorite minerals with W-Cu (Mo) mineralization. Chlorite minerals were identified in each mineralization type for complete structural, chemical and stable isotopic characterization using the same samples for each of these analyses.

Analytical techniques

Optical microscopy

Thin polished sections were prepared for optical microscopy in transmitted and reflected light. Textural relationships between chlorite minerals and opaque minerals (i.e. tungstates and sulfides) were examined using a Nikon E400 polarized transmitted-reflected light microscope using thin polished sections (30 μm).

X-ray diffraction

Chlorite fractions (<2 μm) were separated from bulk-rock mineralized pulps by centrifugation. The oriented specimens of <2 μm fractions prepared on glass slides were analyzed in an air-dried (AD) condition and saturated in ethylene-glycol (EG) vapour for 24 h. Structural characterization of the <2 μm oriented clay-fraction specimens was performed using a Philips X'Pert diffractometer with Cu*K*α radiation and a monochromator, working at 50 kV and 30 mA. A scanning speed of 0.05°2θ/min for the range 2–65°2θ and a counting time of 5 s/step were used. The interlayer nature, the polytype and d_{060} values of the chlorite minerals were examined using randomly oriented specimens. The XRD patterns of these specimens were acquired using a RINTUltima^{+} diffractometer with a Cu X-ray tube, Ni-filter, and silicon strip X-ray detector (Rigaku D/teX Ultra). A measurement condition of 0.25° divergence slit, 10 mm mask confining the beam width, and 8 mm anti-scatter slit was used. The XRD pattern was obtained with a scanning speed of 0.10°2θ/min at a counting time of 20 s/step over the range 2–75°2θ.

EMPA

Quantitative compositions were obtained using an electron microprobe analyser, a JEOL Hyperprobe JXA-8500F operated at 15 kV accelerating voltage and 10 nA beam current for silicates and at 20 kV and 20 nA for tungstates and sulfides. Samples of chlorite with W, (Cu,Mo) mineralization were analysed using doubly polished thick sections (200 μm). The major elements of minerals were determined using detection limits (3σ) of 0.03 wt.% for most oxides with counting times of 80 s. The standards used for silicates were: albite (Na*K*α), orthoclase (Al*K*α, Si*K*α, K*K*α), apatite (Ca*K*α, P*K*α), MgO (Mg*K*α), $MnTiO_3$ (Mn*K*α), TiO_2 (Ti*K*α), FeO (Fe*K*α); for W minerals: cassiterite (Sn*K*α), pure Ta (*L*α), Mo (*L*α), Ni (*K*α), Co (*K*α), Cu (*K*α), Ag (*L*α) and Au (*M*α) metals, SrBa NbO_4O_{12} (Nb*L*α), scheelite (W*L*α), Sc_2O_3 (Sc*L*α), UO_2 (U*M*β), ThO_2 (Th*M*β), galena (Pb*M*α), LaP_5O_{14} (La*L*α), CeP_5O_{14} (Ce*L*α), YAg (Y*L*α), Cd (*L*α), Sb_2S_3 (Sb*L*α), AsGa (As*L*α), Bi_2Se_3 (Bi*M*α). Calculation of the structural formula was based on 28 oxygens for chlorite and on 4 oxygens for the tungstate minerals. The Fe^{3+} estimation in chlorite was carried out according to Droop (1987) and Jacobson (1989).

Oxygen isotopes

Fe-, Fe,Mn- and Fe,Mg-chlorite samples (previously analysed by XRD) were selected for oxygen isotope analyses carried out at the Laboratory for Stable Isotope Science, University of Western Ontario (London, Ontario, Canada). Oxygen isotopic analysis of quartz samples from the W- and Mo-mineralization were analysed at the University of Salamanca (Spain). A conventional procedure was used for the extraction of oxygen from chlorite and quartz with BrF_5 and quantitative conversion to CO_2 prior to analysis by stable-gas mass spectrometry (Clayton and Mayeda, 1963). The $\delta^{18}O$ values are reported in ‰ relative to Vienna-Standard Mean Ocean Water (V-SMOW) and normalized to the

https://doi.org/10.1180/minmag.2017.081.104 Published online by Cambridge University Press

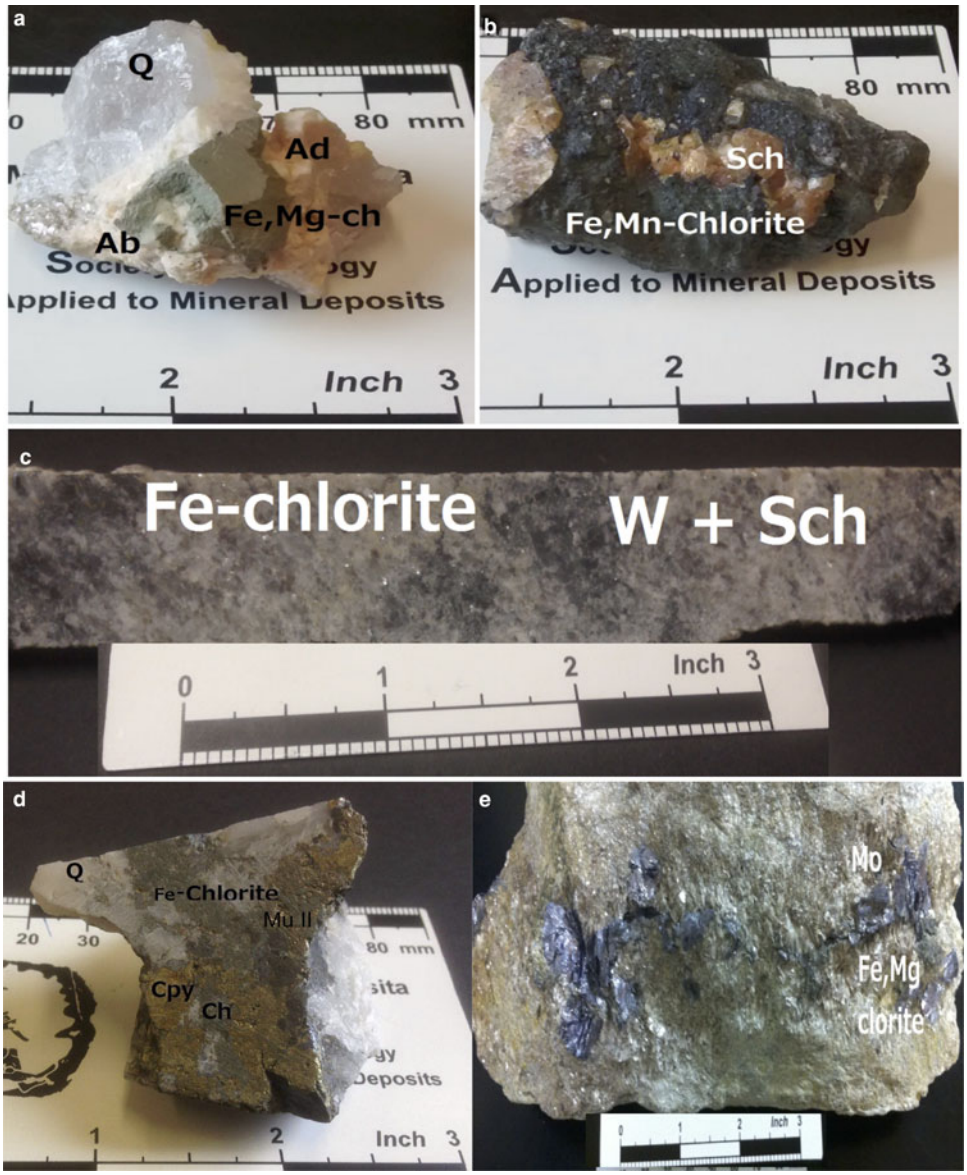

FIG. 3. Selected samples of chlorite minerals studied: (*a*) sample from Santa Helena collected at –48 m: Q – quartz; Ad – adularia; Ab – albite; Fe,Mg-chlorite; (*b*) sample from Santa Helena collected from veins at –148 m: Sch – scheelite; FeMn-chlorite; (*c*) sample collected from the Santa Helena breccia structure (North Sto. António at –160 m): W – wolframite; Sch – scheelite; Fe-chlorite; (*d*) sample from the Santa Helena breccia structure collected at –176 m: cpy – chalcopyrite; chl-Fe-chlorite, Mu II – secondary muscovite; (*e*) sample from Venise collected at –110 m; Mo – molybdenite; Fe,Mg-chlorite.

NBS-30 reference (+5.17‰ *vs.* V-SMOW) and NBS-28 (+9.34‰ *vs.* V-SMOW). The reproducibility of $\delta^{18}O$ measurements is ±0.2‰ (1σ). The following isotope fractionation equations were used here between the mineral and water system: the chlorite–H_2O (Wenner and Taylor, 1971), the quartz–H_2O (Clayton *et al.*, 1972), and albite–H_2O (Matsuhisa *et al.*, 1979).

https://doi.org/10.1180/minmag.2017.081.104 Published online by Cambridge University Press

Results

Macroscopic observations and optical microscopy

Five distinct assemblages of chlorite minerals were identified in the W, (Cu,Mo) ore deposit of Borralha (Fig. 3): (1) quartz + albite + adularia + Fe,Mg-chlorite; (2) Fe,Mn-chlorite + scheelite; (3) Fe-chlorite + wolframite + scheelite; (4) Fe-chlorite + chalcopyrite + sphalerite ± pyrite + secondary muscovite (+ sericite); (5) Fe,Mg-chlorite + molybdenite + bismuthinite ± adularia + quartz. Mg,Fe-chlorite with chalcopyrite was observed by optical and electron microscopy. Chlorite minerals observed in transmitted light were recognized easily by their green pleochroism, varying from pale green for some massive aggregates to dark green with a basal cleavage and anomalous birefringence in cross-polarized light. Under the microscope, Fe,Mn-chlorite is characterized by strong green pleochroism with an atypical dark orange interference (Fig. 4*a*,*b*), which is in accordance with octahedral occupancy by Mn^{2+} (Bailey, 1988). The elongation sign is opposite to the optical sign and the optical plane is almost parallel to (010). The Fe,Mn-chlorite aggregates are larger (800–1500 μm) than those of the Fe-chlorite. Fe-chlorite (Fig. 4*c*,*d*) shows flaky micrometric aggregates with greenish pleochroism and a much lower birefringence compared to Fe,Mn-chlorite. Small flaky aggregates of Mg,Fe-chlorite (Fig. 4*e*, *f*) with chalcopyrite show a randomly oriented grey to pale green pleochroism and small sheet aggregates, <100 μm in size.

Structural data

Oriented specimens of Fe-, Fe,Mn- and Fe,Mg-chlorite were examined both air-dried (AD) and following treatment with ethylene-glycol (EG) vapour (Supplementary material, see below). XRD patterns of the three samples studied show the (00*l*) reflections distinctive of chlorite minerals, where the 002 peak at 7 Å is sharper than the 001 peak at 14 Å and the 001 and 003 peaks show approximately equal intensities. This is a typical structural feature for Fe-chlorite, where a large number of Fe atoms are distributed between the two octahedral sites. The different relative intensities of the 00*l* reflection planes may be used to measure the total metals (e.g. Ni, Co, Cr, Mn) incorporated between the silicate and hydroxide octahedral sheets (Brown and Brindley, 1980). Greater intensities of the 00*l* reflections in Fe,Mn-chlorite are due to the presence of Mn (measured by EMPA) in the octahedral sheet. Increasing the amounts of Fe and Mn in the chlorite structure causes a decrease in the 001, 003 and 005 reflections relative to the 002 and 003 reflections. The normal 001 peak at 14.2 Å occurs at 14.60 Å which is typical of clinochlore (daphnite), or at 14.3 Å for pennantite. This is explained by the presence of the metals in the hydroxide layer and, to a lesser extent, by the presence of a few tri-smectite layers interstratified with tri-chlorite. There is a marked effect of Fe symmetry on the intensity ratio of the 001 and 003 peaks and approximately equal intensities indicate a symmetrical Fe substitution. The 001 and 005 reflections are weak relative to the 003 reflection due to the presence of Fe in the hydroxide layer. After EG treatment the peak positions did not change, but the intensity of the 00*l* peaks decreased. This probably indicates that expandable layers such as those of smectite do not occur in these chlorites although changes in the oxidation state may complicate this issue.

Textural relationships: chlorite vs. mineralization

The areas of the sections examined by means of optical microscopy were selected for detailed subsequent analysis by electron microscopy for to better understand the textural relationships between the chlorite minerals and the oxides or sulfides. Several textural relationships were examined, in particular those involving Fe,Mn-chlorite and scheelite (Fig. 5*a*), Fe-chlorite and wolframite and scheelite (Fig. 5*b*), Fe-chlorite and wolframite (Fig. 5*c*), Fe-chlorite *vs.* wolframite and Mg,Fe-chlorite *vs*. chalcopyrite (Fig. 5*d*), Fe-chlorite + secondary muscovite + chalcopyrite + wolframite (Fig. 5*e*), and Fe,Mg-chlorite along the cleavage planes of molybdenite (Fig. 5*f*).

Crystal chemistry of the chlorite minerals

Fe,Mn-chlorite

The EMPA analyses of Fe,Mn-chlorite (Table 1, analyses 1, 2, see also Supplementary material) show an average crystal chemical composition corresponding to: $(Al_{2.62}Fe_{7.53}Mn_{1.09}Mg_{0.62}Zn_{0.02}Ca_{0.01})_{11.89}(Si_{5.31}Al_{2.69})_8O_{20}(OH)_8$. The Si⇔Al(IV) exchange does not confirm tetrahedral substitution, but there is evidence of R^{2+} exchange (Mn^{2+} for Mg^{2+} or Mn^{2+} for Fe^{2+}) in the octahedral sheet.

https://doi.org/10.1180/minmag.2017.081.104 Published online by Cambridge University Press

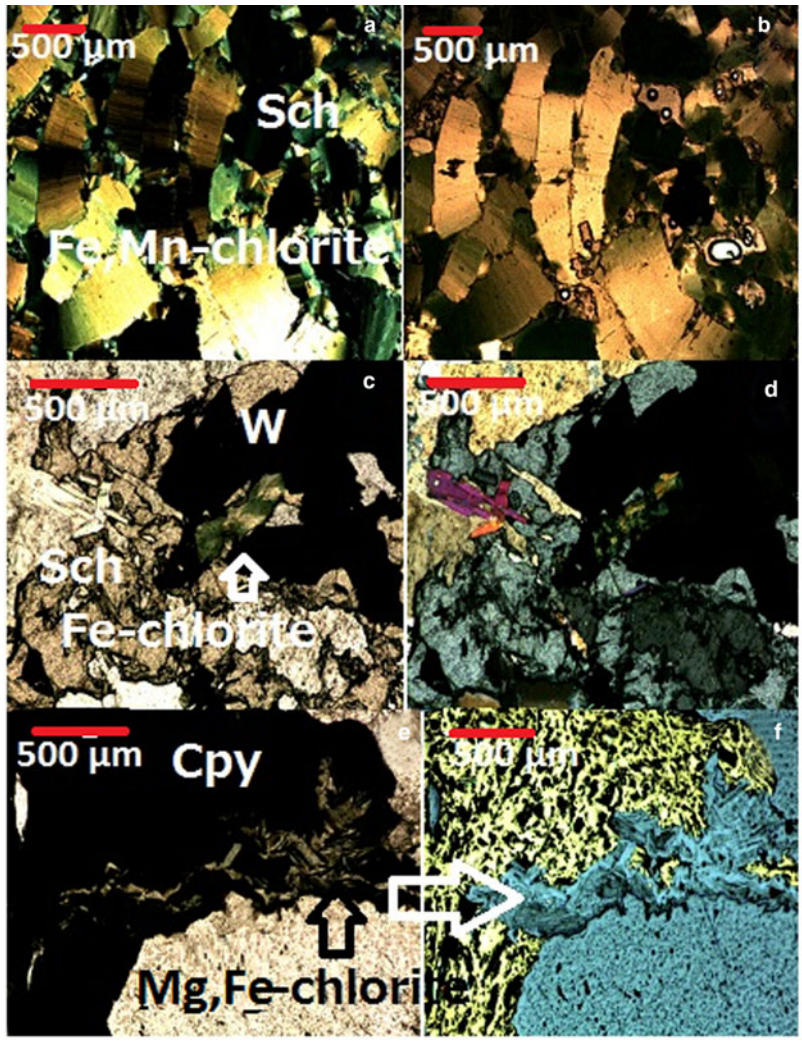

FIG. 4. Photomicrographs showing textural relationships between chlorite and W- and sulfide-mineralization: (*a,b*) Fe, Mn-chlorite and scheelite (*a* = plain polarized light, *b* = crossed nicols); (*c,d*) Fe-chlorite and W mineralization: wolframite (W) and scheelite (Sch) (*c* = plain polarized light, *d* = crossed nicols); (*e,f*) Mg,Fe-chlorite and chalcopyrite (cpy) in reflected light (*e* = plain polarized light, *f* = crossed nicols).

The Fe^{3+} calculated is present in minor amounts. It is assumed here that Fe^{3+} replaces only Al(VI) in the chlorite structure. Small amounts of Zn^{2+}, Ca^{2+}, Na^{+} and K^{+} were identified in Fe,Mn-chlorite. The oxidized chlorites are distinguished by the Si contents of 5.6–6.2 atoms per formula unit (apfu), whereas for the non-oxidized chlorites the Si contents range from 5 to 7 apfu for a maximum of 8 apfu (Deer *et al*., 1976). The Fe/(Fe + Mg) ratio shows an average value of 0.92 (Supplementary material). Compositionally, the Fe,Mn-chlorite falls between daphnite and amesite (see Fig. 11) in the diagram of R^{2+} *vs.* Si^{4+} (Wiewióra and Weiss, 1990).

Fe-chlorite

The EMPA analyses of Fe-chlorite (Table 1, analyses 3, 4; see also Supplementary material) display an average crystal chemical composition of: $(Al_{3.01}Fe^{3+}_{0.25}Fe^{2+}_{7.95}Mn_{0.26}Mg_{0.19})_{11.66}(Si_{5.44}Al_{2.56})_8O_{20}(OH)_8$. Small amounts of Mn and Mg (<0.34 apfu) are present and the Fe/(Fe + Mg) average ratio is ~0.98 (Supplementary material), suggesting an oxidized

https://doi.org/10.1180/minmag.2017.081.104 Published online by Cambridge University Press

state. The chlorite composition corresponds to daphnite. These compositions are similar to those of Fe-chlorite occurring with chalcopyrite and secondary muscovite (sericite) (Figs 3*d* and 5*e*).

Mg,Fe-chlorite

The EPMA analyses (Table 1, analyses 5, 6; see also Supplementary material) show an average chemical composition characterized by small Al and Fe contents: $(Al_{2.63}Fe^{3+}_{0.37}Fe^{2+}_{1.72}\ Mn_{0.01}Mg_{6.40}\ Ca_{0.26})_{11.39}(Si_{6.02}Al_{1.98})_8O_{20}(OH)_8$. This reflects crystallization conditions which are different from those related to the formation of Fe,Mg-chlorite. The Mn^{2+} is ~0.01 apfu and Ca^{2+} ~0.26 apfu, higher than was found in the chlorite samples analysed previously. The Fe/(Fe + Mg) average ratio is ~0.26 (Supplementary material) and the chlorite composition corresponds to pycnochlorite.

Fe,Mg-chlorite

The average crystal chemical composition (Table 1, analyses 7, 8; see also Supplementary material) is $(Al_{2.89}Fe^{3+}_{0.24}Fe^{2+}_{6.42}Mn_{0.21}Mg_{2.08})_{11.84}(Si_{5.21}Al_{2.79})_8\ F_{0.31}O_{20}(OH)_8$. A decrease in the Al, Fe and Mn contents coupled with an increase in the F content is

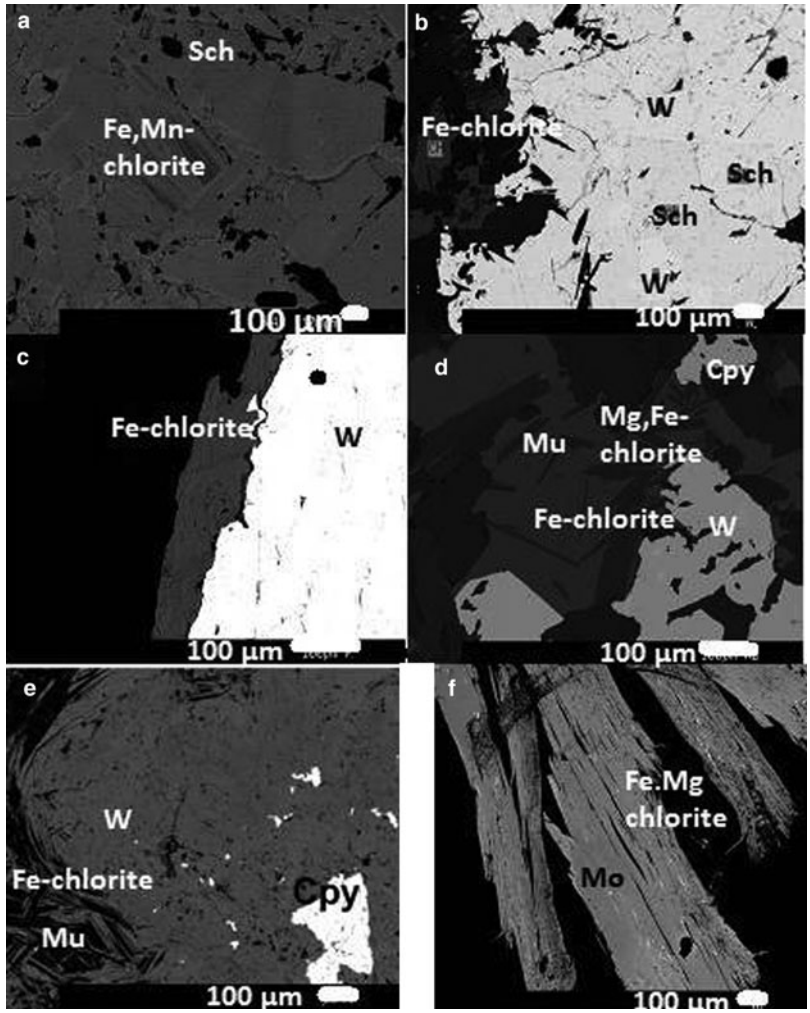

FIG. 5. Back-scattered electron images: (*a*) Fe,Mn-chlorite + scheelite; (*b*) Fe-chlorite + wolframite and scheelite; (*c*) Fe-chlorite and wolframite; (*d*) Fe-chlorite, muscovite (Mu) and wolframite; Mg,Fe-chlorite and chalcopyrite (cpy); (*e*) Fe-chlorite, wolframite and chalcopyrite; (*f*) Fe,Mg-chlorite along the cleavage planes of molybdenite (Mo).

https://doi.org/10.1180/minmag.2017.081.104 Published online by Cambridge University Press

TABLE 1. EMPA results of chlorite and calculated structural formula based on 28 oxygens.

Element	1	2	3	4	5	6	7	8
SiO_2	23.18	22.7	22.74	22.92	30.19	29.19	23.28	23.83
TiO_2	0.08	–	0.02	–	0.02	0.06	0.01	0.01
Al_2O_3	19.88	19.95	20.27	20.64	20.47	20.09	21.02	21.14
FeO	39.52	39.86	42.2	42.54	12.21	13.99	35.57	34.43
MnO	6.23	5.03	1.21	1.33	0.04	0.03	1.06	1.07
MgO	1.87	1.44	0.52	0.45	21.33	19.48	5.9	6.42
CaO	0.04	0.01	0.05	–	1.21	0.96	0.01	0.01
BaO	–	–	–	–	–	–	–	0.08
Na_2O	0.03	0.03	0.06	–	–	–	–	0.01
K_2O	0.01	–	–	–	–	–	–	–
Rb_2O	–	–	–	–	–	–	–	0.03
ZnO	0.11	0.29	–	–	–	–	0.05	–
F	–	–	–	–	–	–	0.25	0.15
Cl	–	–	0.01	–	0.03	–	–	–
Cr_2O_3	–	–	0.02	–	–	–	–	–
CoO	–	–	0.01	0.11	–	–	–	–
Total	90.95	89.31	87.12	87.90	85.50	83.80	87.21	87.24
Si	5.27	5.26	5.35	5.34	5.99	5.97	5.24	5.32
Al(IV)	2.73	2.73	2.65	2.65	2.01	2.03	2.76	2.68
Al(VI)	2.61	2.72	2.99	3.03	2.82	2.85	2.85	2.92
Ti	0.01	–	–	–	–	0.01	–	–
Cr	–	–	–	–	–	–	–	–
Fe^{3+}	–	–	0.18	0.21	0.46	0.47	0.17	0.20
Fe^{2+}	7.56	7.74	8.19	8.08	1.57	1.93	6.53	6.23
Mn	1.20	0.99	0.24	0.26	0.01	0.01	0.20	0.20
Mg	0.63	0.50	0.18	0.15	6.31	5.94	1.98	2.14
Co	–	–	–	0.01	–	–	–	–
Zn	0.02	0.05	–	–	–	–	0.01	–
Ca	0.01	–	0.05	–	0.26	0.21	–	–
Na	0.02	0.02	–	–	–	–	–	0.01
K	–	–	–	–	–	–	–	–
Rb	–	–	–	–	–	–	–	0.01
Ba	–	–	–	–	–	–	–	0.01
F	–	–	–	–	–	–	0.36	0.21
Cl	–	–	0.01	–	0.02	–	–	–
OH	16	16	15.99	16	15.98	15.99	15.64	15.79

Fe^{2+}/Fe^{3+} and OH calculated assuming full site occupancy.
1, 2 Fe,Mn-chlorite (around scheelite crystals).
3, 4 Fe-chlorite (around wolframite and scheelite integrowth).
5, 6 Mg,Fe-chlorite. 7, 8 Fe,Mg chlorite.

clear and it is considered to be a typical feature of this Fe,Mg-chlorite. The Fe/(Fe + Mg) average ratio is ~0.76 (Supplementary material) and the chlorite composition corresponds to that of ripidolite.

X-ray maps of chlorite minerals vs. tungstate and sulfide minerals

X-ray maps illustrate the Fe and Mn distribution and support the notion of chlorite crystallization and metal precipitation directly from the fluid, as discussed below.

Fe,Mn-chlorite

The area illustrated in the inset of Fig. 6 shows Fe, Mn-chlorite associated with scheelite grains. The Fe,Mn and Mg distributions are distinct and reflect the incorporation of Fe followed by Mn. The X-ray maps show the W and Ca distributions in the scheelite (Fig. 7, inset) and the EPMA of the

https://doi.org/10.1180/minmag.2017.081.104 Published online by Cambridge University Press

scheelite (Table 2, analyses 1, 2; see also Supplementary material) indicate traces of Sn, Pb, Bi and Mo.

Fe-chlorite

The area illustrated is a veinlet infill of Fe-chlorite aggregates associated with wolframite (Fig. 8). The X-ray map shows that the Fe distribution in the chlorite aggregates is clearly defined, Mg is limited to the edges of the chlorite aggregates and Mn is confined to the central part of the chlorite (Fig. 8, inset). The EMPA analyses of the wolframite (Table 2, analyses 3, 4; see also Supplementary material) show trace amounts of Nb, Ta, Sn and Ti. The wolframite is not homogeneous revealing variations of in terms of the MnO and FeO composition as reported by Noronha (1983). In contrast to the wolframite from Panasqueira which is enriched in the ferberite component ($FeWO_4$), the hübnerite ($MnWO_4$) component of wolframite is more significant at Borralha (Fig. 9) and as well as in other Iberian tungsten deposits (Neiva, 2008).

Mg,Fe-chlorite

The areas illustrated correspond to chlorite veins close to chalcopyrite. The back-scattered image (Fig. 10, inset) shows aggregates of secondary muscovite (sericite) which may be a greisen-type alteration, and Fe-chlorite associated with wolframite and chalcopyrite. Particular attention was given to the X-ray map of Mg distribution, where small chlorite aggregates associated with chalcopyrite are enriched in Mg (shown in red) at the expense of Fe.

Chlorite geothermometry

Chlorite shows a wide compositional range because it is sensitive to *P-T* and redox conditions, as well as the bulk-rock and fluid composition (Walshe, 1986; Cathelineau, 1988; Vidal *et al*., 2001, 2005, 2006; Inoue *et al*., 2009; Bourdelle *et al*., 2013; Lanari *et al*., 2014). Here we used the geothermometry model of Bourdelle *et al.* (2013) and Bourdelle and Cathelineau (2015) which considers all the iron to be Fe^{2+}. Those authors justified this approach by

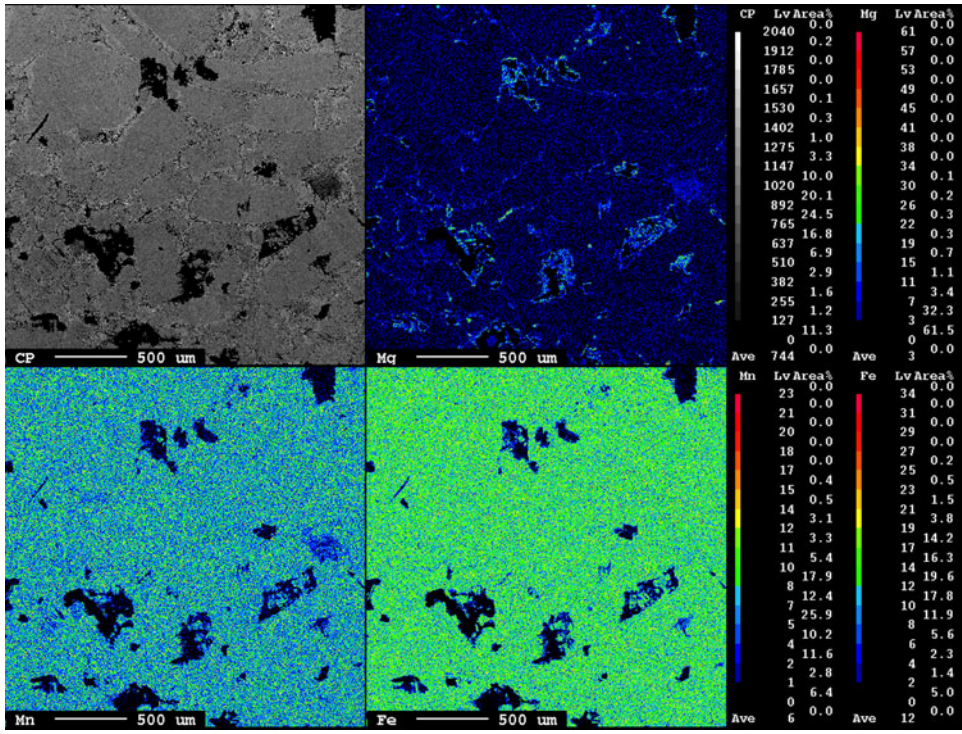

FIG. 6. X-ray maps of Fe, Mn and Mg distributions in Fe,Mn-chlorite. Black areas correspond to scheelite. (CP – composite.)

https://doi.org/10.1180/minmag.2017.081.104 Published online by Cambridge University Press

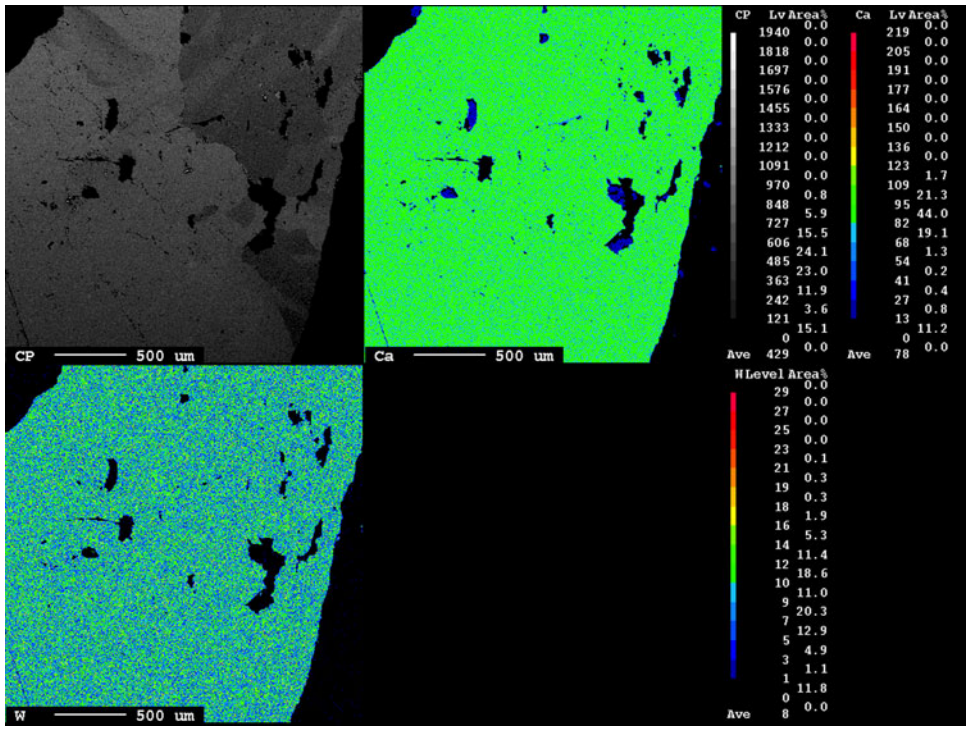

FIG. 7. X-ray maps of Ca and W distributions in scheelite.

the fact that, accounting for Fe^{3+} in the structural formula, fixed numbers of oxygens reduce the number of cations, implying an increase in octahedral vacancies. That in turn creates an indirect link between the Fe^{3+} content and the temperature. The chlorite temperature estimates are controlled in the first place by Tschermak substitution, where Fe^{3+} has a subordinate role that may be disregarded as a first approximation. The mineral compositions were plotted in the Si^{4+} *vs.* R^{2+} diagram (Wiewióra and Weiss, 1990), and four distinct geothermometric fields were (Fig. 11): (1) Fe,Mn-chlorite falls into a field with *T* ranging from 400 to 500°C; (2) Fe-chlorite plots in a field where *T* varies from 250 to 350°C; (3) Fe,Mg-chlorite corresponds to a field with *T* of ~200–250°C; and (4) Mg,Fe-chlorite falls in a field with *T* of ~150°C.

Stable isotope data

Oxygen isotopic measurements of the Fe-, Fe,Mn-, Fe,Mg-chlorites, quartz from W- and Mo-mineralization (Santa Helena and Venise breccia pipes), adularia from the quartz + Fe,Mg-chlorite + molybdenite assemblage and the oxygen isotopic fractionations between chlorite, quartz, adularia and H_2O related to W- and sulfide mineralization are shown in Table 3. These data are compared with the isotopic data for quartz from the Gerês late-orogenic granitic massif (Jaques *et al.*, 2016) and from the Panasqueira deposit (Polya *et al.*, 2000).

The $\delta^{18}O$ isotope (V-SMOW) of the chlorites yielded values of +1.5 (1σ) for (Fe,Mg-chlorite), +3.8 (1σ) for (Fe-chlorite) and +6.91 (1σ) for (Fe, Mn-chlorite). The isotopic fractionation for chlorite and H_2O calculated with the bond-type approach depends on the composition which should be known before interpreting the isotopic data (Cole, 1985, 1994; Savin and Lee, 1988). Oxygen isotopic exchange experiments in the chlorite-H_2O system (Wenner and Taylor, 1971) were calculated assuming a temperature of 200–500°C, inferred from fluid-inclusion studies, and deduced on the basis of chlorite geothermometry according to the procedure described by Bourdelle *et al.* (2013). The $\delta^{18}O_F$ (fluid, *F*) oxygen isotopic fractionation for the chlorite-H_2O pair (Wenner and Taylor, 1971), assuming a temperature of 300°C, yield values (Table 3) for the ancient fluid values of +1.45 (1σ),

https://doi.org/10.1180/minmag.2017.081.104 Published online by Cambridge University Press

TABLE 2. EPMA results from scheelite and wolframite, and calculated structural formulae based on 4 oxygens.

Element	1	2	3	4
WO_3	81.39	81.04	74.41	73.86
CaO	18.78	18.16	0.01	0.02
FeO	–	–	10.69	9.14
MnO	0.08	–	14.31	16.29
TiO_2	–	–	0.01	0.01
Nb_2O_5	–	–	0.38	0.40
Ta_2O_5	–	–	0.05	0.06
SnO_2	–	–	0.03	0.01
MoO_3	0.08	0.06	–	–
Total	100.33	99.29	99.89	99.79
W	1.083	1.089	0.971	0.964
Ca	0.749	0.732	–	–
Fe	–	–	0.450	0.385
Mn	0.003	–	0.575	0.625
Ti	–	–	–	–
Nb	–	–	0.009	0.009
Ta	–	–	0001	0.001
Sn	–	–	–	–
Mo	–	–	–	–
Total	1.835	1.822	2.043	2.055

1, 2 scheelite.
3, 4 wolframite.
Bi, Sc, Th, U, Pb below detection.

+3.75 (1σ) and +6.86 (1σ) in equilibrium with Fe, Mg-, Fe- and Fe,Mn-chlorite, respectively. Assuming a minimum temperature of 400°C for the crystallization of Fe,Mn-chlorite, the calculated $\delta^{18}O_F$ yielded a value of 8.17 (1σ). The $\delta^{18}O_F$ calculated for Fe,Mg-chlorite and Fe-chlorite yielded values of +0.50 (1σ) and +2.80 (1σ) at a temperature of 250°C.

Quartz collected from W-mineralization (Fig. 3*c*, Santa Helena breccia) has $\delta^{18}O$ (V-SMOW) of +12.6 (1σ) and from Mo-mineralization (Fig. 3*a*, Venise breccia) of +11.40 (1σ). The $\delta^{18}O_F$ fractionation for the quartz-H_2O pair (Clayton *et al.*, 1972) yields a value of +5.67 (1σ) and +4.51 (1σ) for the quartz precipitation at 300°C, based on isotope thermometry. Lower values of +3.65 (1σ) and +2.45 (1σ) were obtained for quartz at a temperature of 250°C close to the isotopic values obtained from the ancient fluid responsible for the Fe-chlorite crystallization.

The $\delta^{18}O$ isotopes (V-SMOW) measurement on adularia collected from the Venise breccia (Fig. 3*a*, *e*) yielded a value of +10 (1σ), where the $\delta^{18}O_F$ fractionation for the feldspar-H_2O pair (Matsuhisa *et al.*, 1979) is +1.75 (1σ).

Discussion

Previous studies of the Borralha W, (Cu,Mo) ore deposit have demonstrated a clear relationship between mineralization and chlorite formation, with ripidolite and daphnite intimately associated with the evolving stage of sulfide deposition (Noronha, 1983, 1984*a*,*b*; Mateus, 1985). The progression from tungstate to sulfide deposition coupled with chlorite crystallization identified in this W, (Cu,Mo) ore system, records an unequivocal connection with the chemical evolution of mineralizing fluids along with the declining *P-T* conditions under which the ore-forming processes took place. The following mineral assemblages are well documented: Fe,Mn- and Fe-chlorite crystallize during the W-ore stage, where a Cu contribution was indicated by the presence of chalcopyrite, whereas Fe,Mg- and Mg,Fe-chlorite throughout the sulfide ore stage is characterized by molybdenite, bismuthinite and pyrite assemblages.

Wolframite crystallized from fluids with slightly acid to neutral pH, where WO_4^{2-} is easily complexed with Fe^{2+}, Mn^{2+} and Ca^{2+}. Note that stability of the Fe^{2+} end-member (ferberite) is much more sensitive to the large variation of f_{O_2} than is the Mn^{2+} end-member wolframite (hübnerite); the composition of ferberite might be affected strongly by the oxidation state of the environment (Hsu, 1976). Furthermore, tungsten may be transported in various aqueous solutions under different conditions where the dominant species above 400°C is tungstic acid, whereas HWO_4^- and WO_4^{2-}, and the alkali-tungstate ion pairs are the most stable species at lower temperatures (Higgins, 1985; Wood and Vlassopoulos, 1989).

Experimental studies on the stability of $H_4[Si(W_3O_{10})_4].2H_2O$ at high *P-T* conditions and variable pH in the presence of Fe^{2+}, Mn^{2+} and Ca^{2+} have confirmed the separation of silicotungstic acid under the effect of solution neutralization (Gundlach, 1967) according to the reaction:

$$[Si(W_3O_{10})_4]^{4-} + 12H_2O = [SiO_4]^{4-} + 12[WO_4]^{2-} + 24H^+ \quad (1)$$

Two distinct tungstate *vs*. silicate assemblages are demonstrated by this work: one consists of scheelite and Fe,Mn-chlorite, whereas the other involves

https://doi.org/10.1180/minmag.2017.081.104 Published online by Cambridge University Press

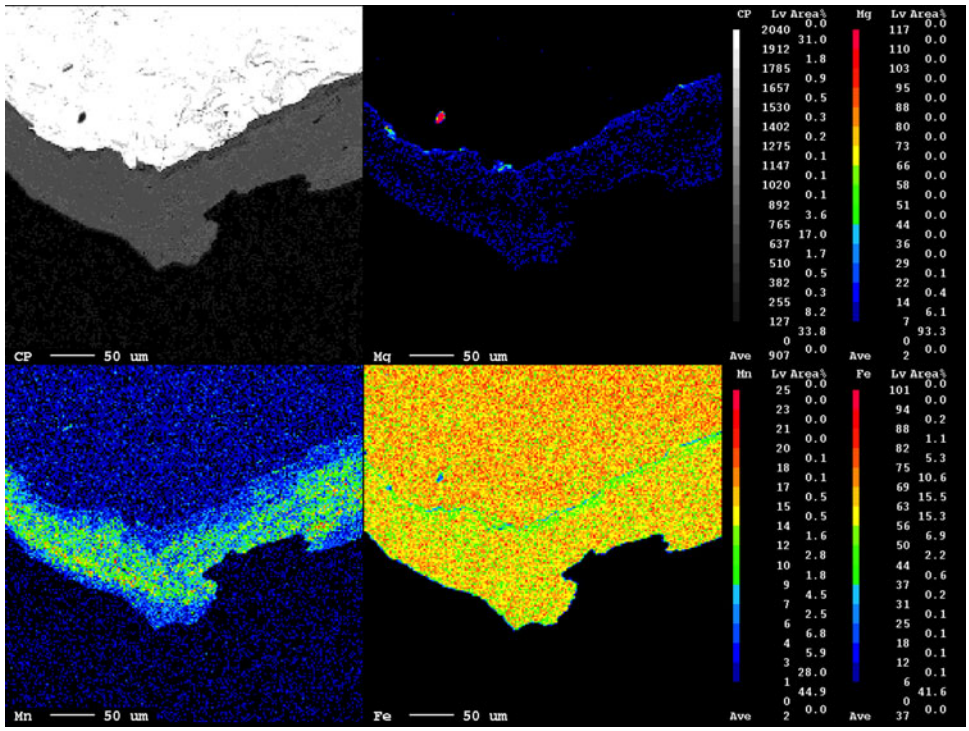

FIG. 8. X-ray maps of Fe, Mn and Mg distributions in Fe-chlorite associated with wolframite.

Mn-rich wolframite ± scheelite + Fe-chlorite. In the first case, $[WO_4]^{2-}$ combined preferentially with Ca^{2+} to form scheelite, favouring the incorporation of the existing Mn^{2+} into the chlorite structure. Crystallization of scheelite together with Mn-bearing wolframite suggests the availability of all three bivalent cations in the hydrothermal fluid. Thus, if Mn^{2+} is partitioned primarily to Mn-bearing wolframite and Ca^{2+} to scheelite, chlorite will be enriched in Fe^{2+} and small amounts of Mn^{2+} (~0.26 apfu) occur in Fe-chlorite, as demonstrated by the Mn-rich wolframite ± scheelite + Fe-chlorite assemblage.

Fe-rich wolframite crystallized in more acidic conditions than did Mn-rich wolframite and scheelite, and the presence of scheelite associated with Mn-rich wolframite, indicate that the minerals are not contemporary. Mn-rich wolframite is associated with a late-evolving W-mineralization stage possibly triggered by rising alkalinity of the fluid as a result of an increase in S activity and the Ca^{2+} availability of the system. This can be correlated with a late alkaline metasomatic reaction which is very common in geochemical settings surrounding the development of W-ore deposits (Wood and Samson, 2000).

The result of $[SiO_4]^{4-}$ and $[WO_4]^{2-}$ separation is direct crystallization of scheelite (I) from the magmatic-hydrothermal fluid and Fe,Mn-chlorite followed by Mn-rich wolframite and scheelite (II) together with Fe-chlorite from the hydrothermal-meteoric fluid. The observed Mn-rich wolframite + scheelite (II) + chalcopyrite assemblage confirms a mixed Mn-rich wolframite-sulfide evolving stage, where scheelite replaced Mn-rich wolframite (seen clearly during optical microscopy) and sulfide minerals precipitated according to the reaction:

$$(Mn, Fe)WO_4 + Ca^{2+}(aq) + 2H_2S(aq) + Cu^{2+}(aq) + O_2 = CaWO_4 + CuFeS_2 + 2H_2O + Mn^{2+} \ldots . \quad (2)$$

The common association of tungstate with some sulfide minerals indicates that sulfur is commonly present and plays a role in the stability of wolframite whereas the stability fields of ferberite ($FeWO_4$) and hübnerite ($MnWO_4$) do not depend

https://doi.org/10.1180/minmag.2017.081.104 Published online by Cambridge University Press

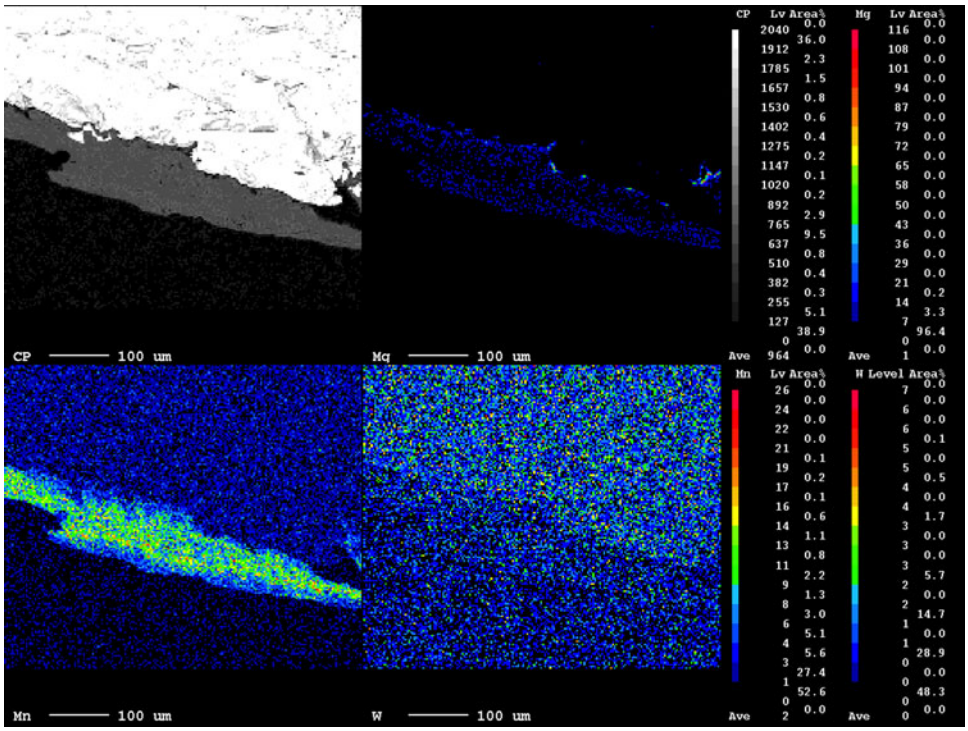

FIG. 9. X-ray maps of Mg, Mn and W distributions in wolframite (hübnerite).

on the presence of oxygen and sulfur (Hsu, 1975). Crystallization of Mg,Fe-chlorite associated with chalcopyrite (Fig. 5*d*) in the Santa Helena breccia, in a mineral assemblage comprising Fe-chlorite, secondary fine-grained muscovite (sericite), Mn-bearing wolframite and scheelite, is particularly interesting. The suite of mineralogical reactions should be expected to begin with the silicates followed by the development of the tungstate minerals. The presence of the chalcopyrite + Mg, Fe-chlorite assemblage suggests that Fe from wolframite was consumed during the crystallization of chalcopyrite, whereas the Mg,Fe-chlorite is a byproduct after the formation of secondary muscovite from biotite according to the reaction:

$$\begin{aligned} &K(Mg, Fe)_3(AlSi_3O_{10})(OH)_2 + 2KAlO_2 + 6HCl \\ &= KAl_2(AlSi_3O_{10})(OH)_2 + 3(Mg, Fe)Cl_2 \\ &\quad + 2K(OH) + 2H_2O \ldots . \end{aligned} \tag{3}$$

In this case, the Mg,Fe-chlorite is not a suitable guide to sulfide mineralization.

Crystallization of Fe,Mg-chlorite associated with molybdenite in the Venise breccia pipe is clearly related to different geochemical conditions imposed by some chemical rejuvenation of hydrothermal fluids, expressed by an increase in f_{S_2} and a pH variation from alkaline to neutral pH. Molybdenite, in contrast to ferberite or hübnerite, crystallized in a more reduced environment according to the reaction:

$$\begin{aligned} 4H_2MoO_4 + 9H_2S = 4MoS_2 + SO_4^{2-} + 2H_3O \\ + 10H_2O \ldots . \end{aligned} \tag{4}$$

This reaction generates more protons in the fluid and produces conditions favourable to the destabilization of primary biotite, and enriching the fluid in Mg^{2+} and Fe^{2+}. Releasing this fluid through the cleavage planes of molybdenite, contributed to the later crystallization of Fe,Mg-chlorite in the system (Fig. 5*f*). The distribution of Fe,Mg-chlorite is widespread and often occurs together with hydrothermal quartz, adularia or secondary albite (Fig. 3*a*) which means that the fluid was widely distributed throughout in the Venise breccia pipe.

The Fe- and Fe,Mn-chlorite is described here associated with W-mineralization for the first time in the magmatic-hydrothermal Borralha system.

https://doi.org/10.1180/minmag.2017.081.104 Published online by Cambridge University Press

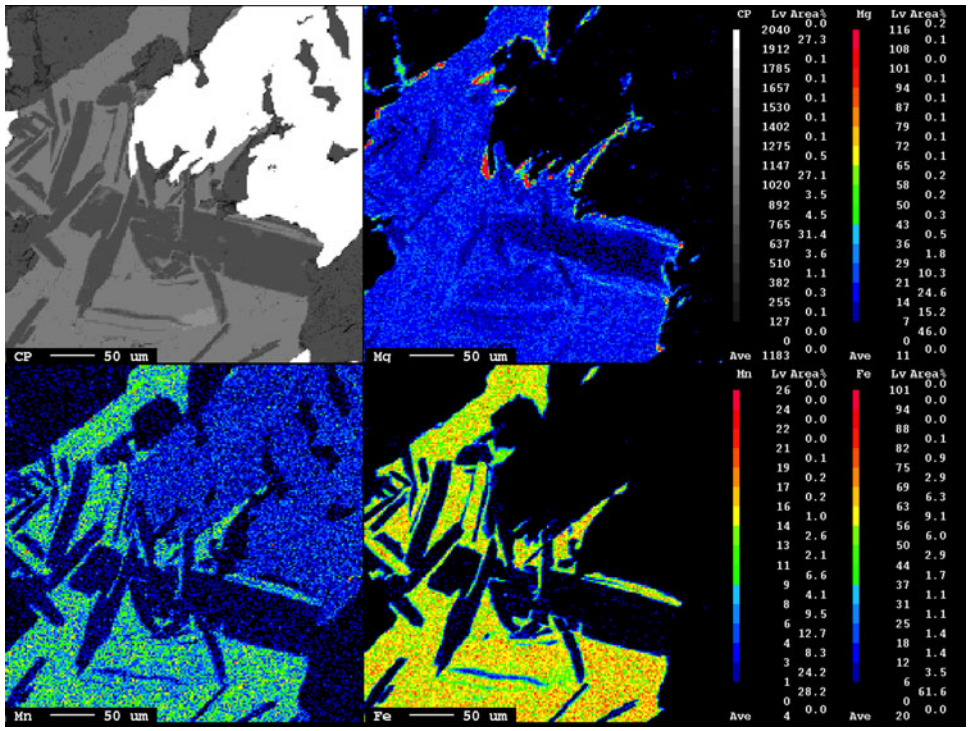

FIG. 10. X-ray maps of Fe, Mn and Mg distributions in Fe-chlorite and Mg,Fe- chlorite (red areas).

The structure and chemistry of the chlorites reveal important details of the conditions of crystallization. The XRD data confirmed that there are no expandable phases in the Fe-, Fe,Mn- or Fe,Mg-chlorite structure, thus making them suitable for geothermometry. The presence of metals (i.e. Mn) in the chlorite structure affected the 002/001 intensity ratios. Large amounts of Fe [Fe/(Fe + Mg + Mn) = 0.4–0.95] and Mn [Mn/(Fe* + Mg) > 0.05] in chlorites are diagnostic of the chemical environments during ore formation (Inoue *et al*., 2010).

The temperatures estimated using the method of Bourdelle *et al.* (2013) indicate three events correlated with the mineralization stages described by Noronha (1983): (1) Early tungsten stage: formation of scheelite (I) and Fe,Mn-chlorite at temperatures from 400 to 500°C; (2) Late tungsten-sulfide stage II: formation of Mn-rich wolframite + scheelite (II) + sulfide (chalcopyrite), and Fe-chlorite and secondary muscovite at 250–350°C; and (3) Sulfide stage III: formation of molybdenite (+bismuthinite) and Fe,Mg-chlorite at ≤250°C.

The $\delta^{18}O_F$ (+6.86 and +8.16 1σ) values calculated (Wenner and Taylor, 1971), responsible for Fe,Mn-chlorite crystallization in the temperature range of 300–400°C, show that the Fe,Mn-chlorite and scheelite (stage I) were likely to have been deposited from magmatic-hydrothermal fluids. The oxygen isotopic results from Fe,Mn-chlorite are very close to those reported by Borsevski *et al*. (1979) for chlorite from Sn-ore deposits in the Transbaikal (Serlovaia Gora and Hapceranga) Russia, where measured values of +6.1 and + 4.4‰ are due to equilibration with a hydrothermal fluid with an isotopic signature of ~+6.05‰.

The temperature estimation of tungsten and sulfide deposition (stage II) based on fluid-inclusion studies of quartz from the Borralha deposit ranges from 270 to 350°C for tungsten associated with aqueous-carbonic fluids with an average salinity of 10 wt.% eq. NaCl; and from 250 to 300°C for chalcopyrite associated with aqueous fluids (Noronha, 1984*b*). Oxygen isotopic results from Fe- and Fe,Mg-chlorite (stage II and III) confirm the same isotopic association between chlorite and the aqueous fluid. Assuming a temperature of ~300°C, the calculated $\delta^{18}O_F$ for the Fe-chlorite-H_2O pair is ~+3.75 (1σ). The $\delta^{18}O$

https://doi.org/10.1180/minmag.2017.081.104 Published online by Cambridge University Press

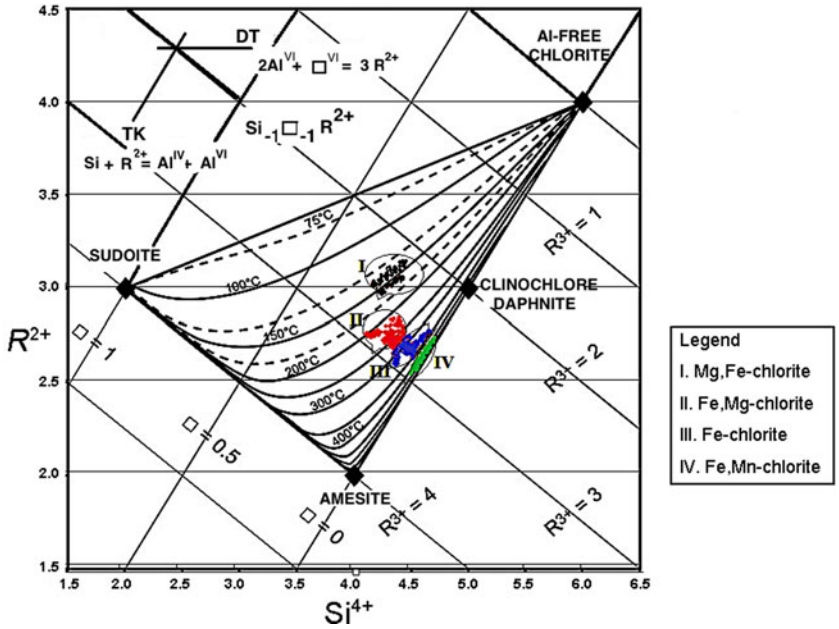

FIG. 11. Projection of chemical compositions of Fe,Mn-chlorite (I), Fe-chlorite (II), Fe,Mg-chlorite (III) and Mg,Fe-chlorite (IV) in the R^{2+}–Si diagram) for chlorite compositions (Wiewióra and Weiss, 1990). The temperature estimation is after Bourdelle *et al*. (2013).

TABLE 3. Oxygen isotope data of chlorite, quartz and adularia from the W, (Cu, Mo) ore deposit of Borralha, Portugal.

Samples	$\delta^{18}O$ (‰) mineral (‰)	$\delta^{18}O_F$(‰) fluid 400°C	$\delta^{18}O_F$(‰) fluid 300°C	δO_F (‰) fluid 250° C	T_h ‡	T (°C) Stable isotope	T (°C) Bourdelle *et al.* (2013)
Fe,Mn-chlorite	6.91	8.17	6.86	–	–	445	480 ± 50
Fe-chlorite	3.80	–	3.75	2.80	–	275	300 ± 50
Fe,Mg-chlorite	1.50	–	1.45	0.50	–	190	225 ± 25
Quartz, W-veins (Santa Helena)	12.60	–	5.67	–	225/246	270	–
Quartz, Mo-veins (Venise)	11.40	–	4.51	3.65	225/246	230	–
Adularia I (Venise)	10.00	–	–	1.75	–	220	–
Adularia II (Venise)	10.00	–	–	1.75	–	220	–
Quartz I (Gerês)*	10.97	–	5.16	–	250	300	–
Quartz I (Gerês)*	9.30	–	3.57	–	250	300	–
Quartz (Panasqueira)**	12.2	–	–	3.80	260 ± 5	275	–
Quartz (Panasqueira)**	12.9	–	–	4.40	258 ± 7	300	–

*After Jaques *et al*. (2016); **After Polya *et al.* (2000); ‡Homogenization temperature (T_h) after Noronha (1984*a*); Jaques *et al.* (2016); Polya *et al.* (2000).

https://doi.org/10.1180/minmag.2017.081.104 Published online by Cambridge University Press

isotopic data obtained on quartz from W (Santa Helena breccia) mineralization yielded a value of +12.6 (1σ), in equilibrium with a calculated $\delta^{18}O_F$ of +5.67 (1σ). Such a $\delta^{18}O_F$ value, quite close to a magmatic-hydrothermal signature, would suggest that quartz and Fe-chlorite formation could be related to a mineral–water system with a mixed contribution from meteoric and magmatic-hydrothermal fluids during the late tungsten-sulfide (II) stage. The $\delta^{18}O$ isotopic data of Fe, Mg-chlorite related to Mo-mineralization (Venise breccia, stage III) is light and close to +1.45 (1σ), assuming a temperature of 190°C where the calculated $\delta^{18}O_F$ is ∼+0.05 (1σ). The estimated temperatures are supported by the geothermometer of Bourdelle *et al.* (2013) for Fe,Mg-chlorite crystallization between 200 and 250°C.

The $\delta^{18}O_F$ fractionation for the feldspar-H_2O pair (Matsuhisa *et al.*, 1979) in the case of adularia yielded a value of +1.75 (1σ) and for the quartz-H_2O pair ∼+4.45 (1σ). The $\delta^{18}O$ values for waters that deposited the latest assemblage of quartz-Fe, Mg-chlorite-adularia range from +0.50 to +4.45 (1σ). Oxygen isotope thermometry of early quartz and adularia indicate equilibrium temperatures of ∼220°C (Matsuhisa *et al.*, 1979).

The isotopic signatures can be compared with the $\delta^{18}O$ data obtained from quartz (episyenitic rocks) from the post-D_3 Hercynian granite of Gerês, which revealed values of ∼+10.97‰ ± 1.9‰, in equilibrium with an aqueous fluid where the calculated $\delta^{18}O_F$ is ∼+5.16‰ (Jaques *et al.*, 2016). $\delta^{18}O$ values of 10 and 11‰ have been determined for other granites in the Portuguese Hercynian rocks (Reavy *et al.*, 1991).

Magmatic quartz from the Panasqueira (Portugal) W-ore, has a high $\delta^{18}O$ value of ∼+13‰ and the $\delta^{18}O$ value of primary magmatic waters is +11 ± 1‰ (Kelly and Rye, 1979). The fluids responsible for ore formation exhibited relatively constant fluid inclusion homogenization temperatures (254–260°C) with salinities of 7.4–8.7 wt.% NaCl equivalent and a calculated fluid $\delta^{18}O$ with values from 3.8 to 4.4‰ (Polya *et al.*, 2000). This means, that the ore-forming stage fluid can be explained by isotopic exchange of meteoric waters equilibrated with granite at ∼350°C (Polya, 1989).

Conclusions

Chlorite minerals may indicate enriched, and economically more favourable, hydrothermal systems. The samples studied show a genetic link between Fe-, Fe,Mn- and Fe,Mg-chlorite and W- and Mo-mineralization supported by textural relationships, geothermometry and isotopic signatures. The composition of chlorite was influenced directly by thermal gradients developed during different stages of the mineralizing process in the Borralha magmatic-hydrothermal system. The identification of a possible hydrothermal alteration halo was not possible, but the chlorite phases associated with W- and Cu,Mo-mineralization are an excellent indicator which help to identify the direction in which the mineralized area may be found and a means of estimating the crystallization temperature of chlorite and tungstate or sulfide.

Acknowledgements

The present study was developed in the context of the NEWORES-ERAMIN project financed by FCT-Lisbon, Portugal. The manuscript benefitted from thoughtful reviews by K. Sundblad (Univ. of Turku), K. Billström, (Univ. of Lund) and R. Törnroos (Univ. of Helsinki) which greatly improved the final version. The authors gratefully acknowledge J.F.W. Bowles for editorial handling. Thanks are also due to F. Guimarães (LNEG-Porto, EMPA facility), S. Leal (geological map design), and V. Ramos (photomicrographs). The authors thank Eric O'Brien for help with the English.

Supplementary material

To view Supplementary material for this article, please visit https://doi.org/10.1180/minmag.2017.081.104

References

Bailey, S.W. (1988) Clinochlores: structures and crystal chemistry. Pp. 398–404 in: *Hydrous Phyllosilicates* (S. W. Bailey, editor). Reviews in Mineralogy, **19**, Mineralogical Society of America, Washington, DC.

Borsevski, I.A., Dolomanova, E.I., Lisovskaia, O.I., Medvedovskaia, N.I. and Rojdestvenskaia, I.V. (1979) *Usloviia formirovaniia mineralnih assotiatii olovorudnih mestorojdenii Zabaikala po izotopno-kislorodnIm dannim*. Novie dannîe o mineralah, Izd Nauka, Moskva, 207 pp.

Bourdelle, F. and Cathelineau, M. (2015) Low-temperature chlorite geothermometry: a graphical representation based on a T–R^{2+}–Si diagram. *European Journal of Mineralogy*, **27**, 617–626.

Bourdelle, F., Parra, T., Chopin, C. and Beyssac, O. (2013) A new chlorite geothermometer for diagenetic to low-

https://doi.org/10.1180/minmag.2017.081.104 Published online by Cambridge University Press

grade metamorphic conditions. *Contributions to Mineralogy and Petrology*, **165**, 723–735.

Brown, G. and Brindley, W.G. (1980) X-ray diffraction procedures for clay minerals identification. Pp. 305–361 in: *Crystal Structures of Clay Minerals and their X-ray Identification* (W.G. Brindley and G. Brown, editors). Monograph **5**, Mineralogical Society, London.

Cathelineau, M. (1988) Cation site occupancy in chlorites and illites as a function of temperature. *Clay Minerals*, **23**, 471–485.

Cathelineau, M. and Nieva, D. (1985) A chlorite solid solution geothermometer the Los Azufres (Mexico) geothermal system. *Contributions to Mineralogy and Petrology*, **91**, 235–244.

Cheilletz, A. and Giuliani, G. (1982) Role de la déformation du granite dans la genèse des episyénites feldspathiques des massifs de Lovios-Geres (Galice) et des Zaer (Maroc Central). *Mineralium Deposita*, **17**, 387–400.

Chinchilla, D., Arroyo, X., Merinero, R., Piña, R., Nieto, N., Ortega, L., and Lunar, R. (2016) Chlorite geothermometry applied to massive and oscillatory-zoned radiated Mn-rich chlorites in the Patricia Zn-Pb-Ag epithermal deposit (NE, Chile). *Applied Clay Science*, **134**, 210–220.

Clayton, R.N. and Mayeda, T.K. (1963) The use of bromide pentafluoride in the extraction of oxygen from oxides and silicates for isotopic analysis. *Geochimica et Cosmochimica Acta*, **27**, 43–52.

Clayton, R.N., O'Neil, J.R. and Mayeda, T.K. (1972) Oxygen isotope exchange between quartz and water. *Geophysical Research*, **77**, 3057–3067.

Cole, D.R. (1985) A preliminary evaluation of oxygen isotopic exchange between chlorite–water. *Geological Society American Annual Meeting*, **17**, p. 550.

Cole, D.R. (1994) Evidence for oxygen isotope disequilibrium in selected geothermal and hydrothermal ore deposit system. *Chemical Geology*, **111**, 283–296.

Cooke, D.R., Hollings, P., Wilkinson, J.J. and Tosdal, R. M. (2014) Geochemistry of porphyry deposits. Pp. 357–381 in: *Treatise on Geochemistry* (H.D. Holland and K.K. Turekian, editors). **13**. Elsevier, Oxford.

Deer, W.A., Howie, R.A. and Zussman, J. (1976) *Rock-Forming Minerals: Sheet Silicates*. Longman Group, London, 270 pp.

Dias, R. and Ribeiro, A. (1995) The Ibero-Armorican Arc: a collision effect against an irregular continent? *Tectonophysics*, **246**, 113–128.

Dora, M.L. and Randive, K.R. (2015) Chloritisation along the Thanewasna shear zone, Western Bastar Craton, Central India: Its genetic linkage to Cu–Au mineralisation. *Ore Geology Review*, **70**, 151–172.

Droop, G.T.R. (1987) A general equation for estimating Fe^{3+} concentrations in ferromagnesian silicates and oxides from microprobe analyses, using stoichiometric criteria. *Mineralogical Magazine*, **51**, 431–435.

Ferreira, N., Iglesias, M., Noronha, F., Pereira, E., Ribeiro, A. and Ribeiro, M.L. (1987) Granitoides da Zona Centro Ibérica e seu enquadramento geodinâmico. Pp. 37–51 in: *Geologia de los granitoides y rocas asociadas del Macizo Hesperico* (F. Bea, A. Carnicero, J. Gonzalo, M. Lopez Plaza and M. Rodriguez Alonso, editors). Editorial Rueda, Madrid (Libro de Homenaje a García de Figuerola LC).

Gundlach, H. (1967) Transport und abscheidungsbedingungen von wolframerzen aus wässerigenlisunge. In: *Pegmatische Lagerstätten und lhre wirtschaftliche bedeutung*, H-19, Clausthal - Zellerfeld.

Gustafson, D.L. and Hunt, J.P. (1975) The porphyry copper deposit at El Salvador, Chile. *Economic Geology*, **70**, 857–912.

Higgins, N.C. (1985) Wolframite deposition in a hydrothermal vein system: the Gray River tungsten prospect, Newfoundland, Canada. *Economic Geology*, **80**, 1297–1327.

Hsu, L.C. (1975) Effects of oxygen and sulfur fugacities on the scheelite-tungstenite and powellite-molybdenite stability relations. *Geological Society of America Abstract Program*, **7**, 1123.

Hsu, L.C. (1976) The stability relations of the wolframite series. *American Mineralogist*, **61**, 944–955.

Inoue, A., Meunier, A., Patrier-Mas, P., Rigault, C., Beaufort, D. and Vieillard, P. (2009) Application of chemical geothermometry to low-temperature trioctahedral chlorites. *Clays and Clay Minerals*, **57**, 371–382.

Inoue, A., Kurokawa, K. and Hatta, T. (2010) Application of chlorite geothermometry to hydrothermal alteration in Toyoha geothermal system, southwestern Hokkaido, Japan. *Resources Geology*, **60**, 52–70.

Jacobson, C.E. (1989) Estimation of Fe^{3+} from electron microprobe analyses: observations on calcic amphibole and chlorite. *Journal of Metamorphic Geology*, **7**, 507–513.

Jaques, L., Noronha, F., Liewig, N. and Bobos, I. (2016) Paleofluids circulation associated with the Gerês late-orogenic granitic massif, northern Portugal. *Chemie der Erde*, **76**, 659–676.

Kelly, W.C. and Rye, R.O (1979) Geologic, fluid inclusions, and stable isotope studies of the tin-tungsten deposits of Panasqueira, Portugal. *Economic Geology*, **74**, 1721–1822.

Lanari, P., Wagner, T. and Vidal, O. (2014) A thermodynamic model for di-trioctahedral chlorite from experimental and natural data in the system MgO–FeO–Al_2O_3–SiO_2–H_2O: applications to P–T sections and geothermometry. *Contributions to Mineralogy and Petrology*, **167**, 968–984.

Lowell, J.D. and Guilbert, J.M. (1970) Lateral and vertical alteration–mineralization zoning in porphyry ore deposits. *Economic Geology*, **65**, 373–408.

Mateus, A. (1985) *Characterization of hydrothermal alteration from the W-ore deposit of Borralha*

https://doi.org/10.1180/minmag.2017.081.104 Published online by Cambridge University Press

(Portugal). Report (in Portuguese), Faculdade de Ciências, Universidade de Lisboa, 186 pp.

Matsuhisa, Y., Goldsmith, J.R. and Clayton, R.N. (1979) Oxygen isotopic fractionation in the system quartz-albite-anorthite-water. *Geochimica et Cosmochimica Acta* **43**, 1131–1140.

Matte, P. (1991) Accretionary history and crustal evolution of the Variscan Belt in Western Europe. *Tectonophysics*, **196**, 309–337.

Meinert, L. (1992) Skarns and skarn deposits. *Geoscience Canada*, **19**, 145–162.

Moura, A., Dória, A., Neiva, A.M.R., Leal Gomes, C. and Creaser, R.A. (2014) Metallogenesis at the Carris W-Mo-Sn deposit (Gerês, Portugal): Constraints from fluid inclusions, mineral geochemistry, Re-Os and He-Ar isotopes. *Ore Geology Reviews*, **56**, 73–93.

Neiva, A.M.R. (2008) Geochemistry of cassiterite and wolframite from tin and tungsten quartz veins. *Ore Geology Review*, **33**, 221–238.

Noronha, F. (1983) *Metallogenic study of the W-ore deposit of Borralha*. PhD thesis (in Portuguese). Universidade do Porto, 413 pp.

Noronha, F. (1984*a*) Caractéristiques physico-chimiques des fluides associés à la génese du gisement de tungsten de Borralha (Nord Portugal). *Bulletin de Minéralogie*, **107**, 273–284.

Noronha, F. (1984*b*) Mineralizações espacial e geneticamente associadas ao maciço granítico da Serra do Gerês. *Cuadernos do Laboratorio Xeolóxico de Laxe*, **7**, 87–99.

Noronha, F. and Ribeiro, M.L. (1983) Carta Geológica de Portugal na escala 1/50 000. Notícia Explicativa da Folha 6-A, Montalegre. *Serviços Geológicos de Portugal*, 30 pp.

Noronha, F., Ramos, J.M.F., Rebelo, J., Ribeiro, A. and Ribeiro, M.L. (1981) Essai de corrélation des phases de déformation hercyniennes dans le NW de la Péninsule Ibérique. *Leidse Geologische Mededelingen*, **52**, 89–91.

Noronha, F., Vindel, E., López, J.A., Dória, A., García, E., Boiron, M.C. and Cathelineau, M. (1999) Fluids related to tungsten ore deposits in Northern Portugal and Spanish Central system: a comparative study. *Revista Sociedad Geologica España*, **12**, 397–403.

Noronha, F., Cathelineau, M., Boiron, M.C., Banks, D., Dória, A., Ribeiro, M.A., Nogueira, P. and Guedes, A. (2000) A three stage fluid flow model for Variscan gold metallogenesis in northern Portugal. *Journal of Geochemical Exploration*, **71**, 209–224.

Polya, D.A. (1989) Chemistry of the main stage ore-forming fluids of the Panasqueira W-Cu(Ag)-Sn deposit, Portugal: implications for models of ore genesis. *Economic Geology*, **84**, 497–503.

Polya, D.A., Foxford, K.A., Stuart, F., Boyce, A. and Fallick, A.E. (2000) Evolution and paragenetic content of low δD hydrothermal fluids from the Panasqueira W-Sn deposit, Portugal: new evidence from microthermometric, stable isotope, noble gas and halogen analyses of primary fluid inclusions. *Geochimica et Cosmochimica Acta*, **64**, 3357–3372.

Reavy, R.J., Stephens, W.E., Fallick, A.E., Halliday, A.N., and Godinho, M.M. (1991) Geochemical and isotopic constraints on petrogenesis: The Serra da Freita pluton, a typical granite body from the Portuguese Hercynian collision belt. *Geological Society of America Bulletin*, **103**, 392–401.

Ribeiro, A. (1974) Contribuition à l'étude tectonique de Trás-os-Montes Oriental. *Comunicações dos Serviços Geológicos de Portugal*, **24**, 1–168.

Ribeiro, A., Pereira, E. and Dias, R. (1990) Structure in the Iberian Peninsula. Pp. 220–236 in: *Pre-Mesozoic Geology of Iberia* (R.D. Dallmeyer and G. Martinez editors). Springer-Verlag, Berlin.

Ribeiro, A., Munhá, J., Dias, R., Mateus, A., Peirera, E., Ribeiro, L., Fonseca, P., Araújo, A., Oliveira, T., Romão, J. *et al.* (2007) Geodynamic evolution of the SW Europe Variscides. *Tectonics*, **26**, 1–24.

Savin, S.M. and Lee, M. (1988) Isotopic studies of phyllosilicates. Pp. 189–223 in: *Hydrous Phyllosilicates (Exclusive Micas)* (S.W. Bailey, editor). Reviews in Mineralogy, **19**, Mineralogical Society of America, Washington, D.C.

Sillitoe, R.H. (2000) Gold-rich porphyry deposits: descriptive and genetic models and their role in exploration and discovery. *Society of Economic Geologists Reviews* **13**, 315–345.

Sillitoe, R.H. (2010) Porphyry copper systems. *Economic Geology*, **105**, 3–41.

Vidal, O., Parra, T. and Trotet, F. (2001) A thermodynamic model for Fe–Mg aluminous chlorite using data from phase equilibrium experiments and natural pelitic assemblages in the 100 to 600°C, 1 to 25 kbar range. *American Journal of Science*, **301**, 557–592.

Vidal, O., Parra, T. and Vieillard, P. (2005) Thermodynamic properties of the Tschermak solid solution in Fe-chlorite: application to natural examples and possible role of oxidation. *American Mineralogist*, **90**, 347–358.

Vidal, O., de Andrade, V., Lewin, E., Muñoz, M., Parra, T. and Pascarelli, S. (2006) P-T-deformation-Fe^{3+}/Fe^{2+} mapping at the thin section scale and comparison with XANES mapping: application to a garnet-bearing metapelite from the Sambagawa metamorphic belt (Japan). *Journal of Metamorphic Geology*, **24**, 669–683.

Walshe, J.L. (1986) A six-component chlorite solid solution model and the conditions of chlorite formation in hydrothermal and geothermal systems. *Economic Geology*, **81**, 681–703.

Wenner, D.B. and Taylor, H.R. Jr (1971) Temperatures of serpentinization of ultramafic rocks based on $^{18}O/^{16}O$ fractionation between coexisting serpentine and magnetite. *Contributions to Mineralogy Petrology*, **32**, 165–168.

https://doi.org/10.1180/minmag.2017.081.104 Published online by Cambridge University Press

Wiewióra, A. and Weiss, Z. (1990) Crystallochemical classifications of phyllosilicates based on the unified system of projection of chemical composition: II. The chlorite group. *Clay Minerals*, **25**, 83–92.

Wilkinson, J.J., Zhaoshan Chang, Z., Cooke, D.R., Baker, M.J., Wilkinson, C.C., Inglis, S., Chen, H. and Gemmell, J.B. (2015) The chlorite proximitor: A new tool for detecting porphyry ore deposits. *Journal of Geochemical Exploration*, **152**, 10–26.

Wood, S.A. and Samson, I.M. (2000) The hydrothermal geochemistry of tungsten in granitoid environments: I. Relative solubilities of ferberite and scheelite as a function of T, P, pH and m_{HCL}. *Economic Geology*, **95**, 143–182.

Wood, S.A. and Vlassopoulos, D. (1989) Experimental determination of the hydrothermal solubility and speciation of tungsten at 500°C and 1 Kb. *Geochimica et Cosmochimica Acta*, **53**, 303.

https://doi.org/10.1180/minmag.2017.081.104 Published online by Cambridge University Press